# Development Of An Implantable Trapezium Replacement For Measuring *In Vivo* Loads At The Base Of The Thumb

J.J. Trey Crisco, Julia A. Henke, Daniel McDermott, Rohit Badida, Amy M. Morton, Josephine M. Kalshoven, Douglas C. Moore

UNIVERSITY ORTHOPEDICS
BROWN Department of Orthopaedics
Lifespan Orthopedics Institute
Rhode Island Hospital • The Miriam Hospital
Newport Hospital
*Delivering health with care®*

## Introduction & Aim

The thumb is a common site for trauma and repetitive workplace injury, often leading to the development of osteoarthritis, with altered joint loading a primary mechanism for these pathologies. However, the *in vivo* loads at the joints are not known. The aim for this project was to design and assess the feasibility of an instrumented replacement trapezium capable of measuring loads *in vivo*.

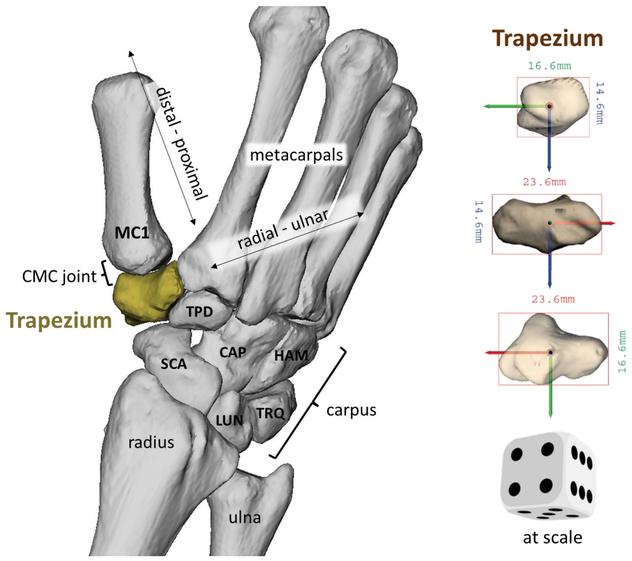


**Fig. 1**. CT derived anatomy of the wrist and trapezium carpal bone (left) and average bounding box dimensions (right).

## Methods

- Two sensor designs were evaluated: Tube and Diaphragm (Fig. 2)
- Tube: 9 strain gauges (120 Ω, VPG Sensors)
- Diaphragm: 5 strain gauges (1000 Ω, VPG Sensors)
- Calibration Testing
  - Gold Standard: 6 DOF load cell (Resolution: 0.25 N and 0.005 Nm. SI 580-20, ATI, Apex, NC)
  - Applied loads: Tube and Diaphragm, respectively, Fx: 48.8, 65.1, Fy: 125.4, 68.6, Fz: 15.8, 53.4, Mx: 0.97, 0.28, My: 0.42, 0.04, and Mz: 0.71, 0.26 (N and Nm)
  - Least Squares (Mat) and Supervised neural network (Deep) with two cascade-forward nets (Levenberg-Marquardt and Bayesian Regularization training functions for forces and moments, respectively), 70/30 train/test and 10k-fold validation on 68,228 and 444,335 data points, respectively. Strain gage failure was modeled by gage data removal.
  - Loading along the longitudinal axis of the first metacarpal (Fy) was set as the most critical outcome measure (x: volar, z: radial).
  - Accuracy was defined as the 95% CI of the limits of agreement (LOA) referenced to the 6 DOF load cell using a Bland-Altman analysis.

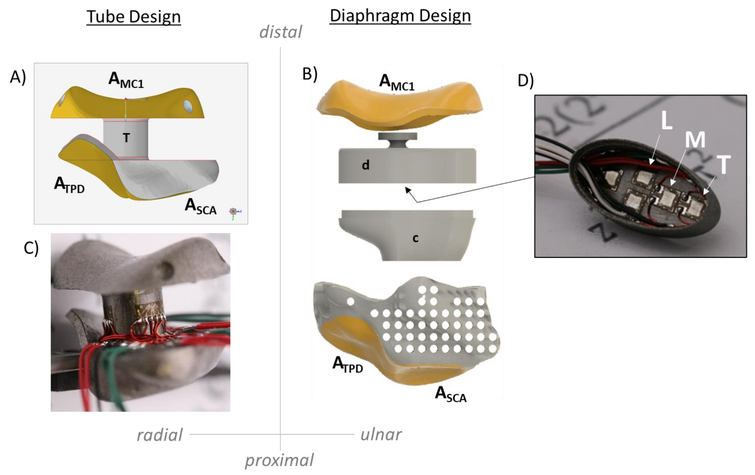


**Fig. 2**. The initial Tube (A & C) and Diaphragm (B & D) designs. The Tube design is based upon the approach previously developed for the knee, hip and shoulder, with gages on a central post (C). The Diaphragm design has strain gages on the underside of a flat, flexible membrane (D). Here, we report data from the left, middle and top strain gauges (L, M, T). Both designs incorporate polished surfaces for articulation with the MC1 ($A_{MC1}$), scaphoid ($A_{SCA}$) and trapezoid ($A_{TPD}$).

## Results

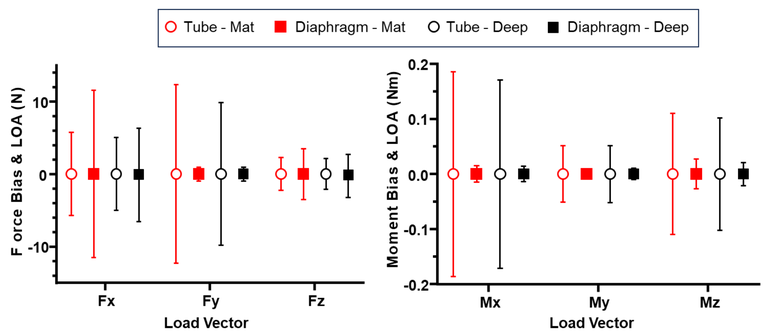


**Fig. 3**. Minimal differences in LOA between Mat and Deep calibration algorithms. The 95% CI LOA in Fy was significantly smaller in the Diaphragm design (1.9 N) than in the Tube design (19.7 N).

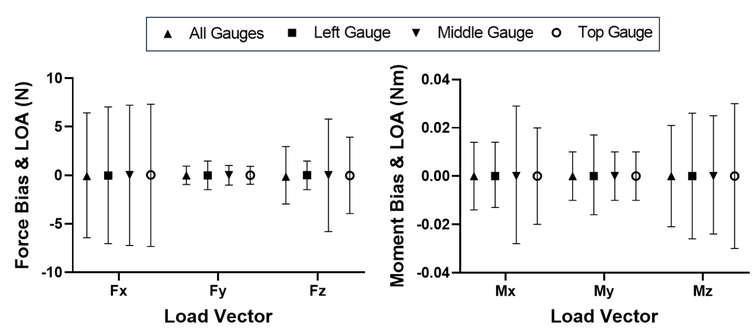


**Fig. 4**. Strain gauge removal had variable effects, depending on sensor design and the number and locations of the gauges removed. For example, removing individual gauges in the Diaphragm design increased the 95% CI LOA for Fy by 3.0 N, 3.9 N, and 5.0 N, for three instances of individual gauge removal, respectively. On the other hand, removal of 2 of the 9 gauges in the Tube design (separately) increased the 95% CI LOA for Fy to 25.8 N and 28.1 N.

## Discussion & Conclusions

There were no notable differences in performance of the Tube and Diaphragm designs. While the tube design has been used successfully in knee, hip and shoulder implants, the small size of the trapezium bone, makes encapsulation of the electronics extremely challenging. Additionally, a trapezium implant can only be secured via soft tissue fixation, as opposed to bone fixation in those larger joints. The Diaphragm design solves this problem. Thus, we are moving ahead with the diaphragm design instrumented with 5 strain gauge, with the goal of measuring loads across the thumb carpometacarpal joint *in vivo,* given its ability to measure axial loads with a 95% CI LOA of approximately 2 N. Many challenges remain before the device can be considered for FDA clearance and implantation in live humans. To minimize subject risk, the device will not be provided with a battery. The power and data systems (BLE) are being developed and evaluated first in benchtop testing, followed by the miniaturization and installation of the components within the Diaphragm on a flexible circuit board. Mechanical components (fabricated from titanium (Ti6Al4V) will be welded and hermetically sealed, followed by fatigue testing for structural and electrical integrity.

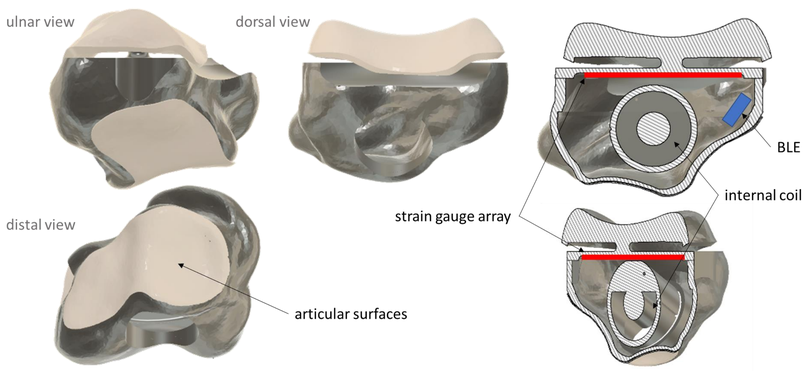


**Fig. 5**. CAD renderings of the current design. The articular surfaces will be polished and hardened with ion implantation. Power will be delivered inductively, via an external coil embedded in a glove. Load and temperature data will be transferred via Bluetooth Low Energy (BLE).

## Significance

An instrumented trapezium capable of measuring loads at the base of the thumb will be immensely valuable to clinicians, researchers, and implant designers who need accurate load data to understand the role of joint loading in thumb pathophysiology, to refine musculoskeletal models, to standardize pre-clinical testing for devices seeking FDA clearance, and to develop more effective and cost-effective surgical treatments.

## Acknowledgements

This research was funded in part by NIH/NIAMS R21AR077201

# ACL-Reconstructed Patients Land in a Higher Injury Risk Position

[1] Beveridge, JE, [1] Hague, M, [1] Parola, LR, [1] Costa, MQ, [2] Molino, J, [1] Fleming, BC.

1. RIH Department of Orthopaedics Bioengineering Lab; 2. Lifespan Biostatics, Epidemiology, Research Design, & Informatics Core

jillian_beveridge@brown.edu

UNIVERSITY ORTHOPEDICS

BROWN Department of Orthopaedics

Lifespan Orthopedics Institute
Rhode Island Hospital • The Miriam Hospital
Newport Hospital
*Delivering health with care®*

## Introduction

- Anterior cruciate ligament (ACL) injury is thought to occur when the knee is at full extension and the tibia translates anteriorly.[1]
- Contralateral ACL injury risk increases after initial injury,[2] as does the risk for post-traumatic osteoarthritis (PTOA).
- ACL reconstruction (ACLR) surgery is the standard of care, but it does not reduce risk of either reinjury, contralateral injury, or PTOA.[3]
- Restoring knee kinematics (motion) and lower limb strength symmetry are goals of ACLR rehabilitation programs;[4] the presence and consequences of chronic asymmetry are unknown.

## Aims & Hypotheses

**Aim:** Quantify bilateral knee kinematics during a dynamic hop landing in ACLR patients and healthy, uninjured persons.

**Hypothesis 1:** ACLR patients will have greater anterior tibial translation at ground contact than healthy control subjects.

**Hypothesis 2:** Hop landing knee position is symmetrical in healthy controls, whereas ACL patients exhibit asymmetry in anterior tibial position with the surgical limb having the greatest abnormality.

## Methods

**Subjects:** 21 patients recruited from an ongoing longitudinal clinical trial examining patient outcomes after ACLR (NCT00434837):[5]

- 10 ACLR patients: 5 females/5 males; 33.8±10.0 years old; BMI = 26.9±4.2; 12.1±1.2 years follow-up).
- 11 Control subjects: 5 females/6 males; 38.1±7.5 years old; BMI = 24.3±3.2; 11.9±3.8 years post initial trial enrollment.

**Knee Kinematics Recording:**

- Biplane videoradiography (BVR) was used to capture knee kinematics with an accuracy of ~0.5°/mm[6] while subjects performed a dynamic 1-leg hop activity that challenges the knee. (Fig 1)

## Methods (continued)

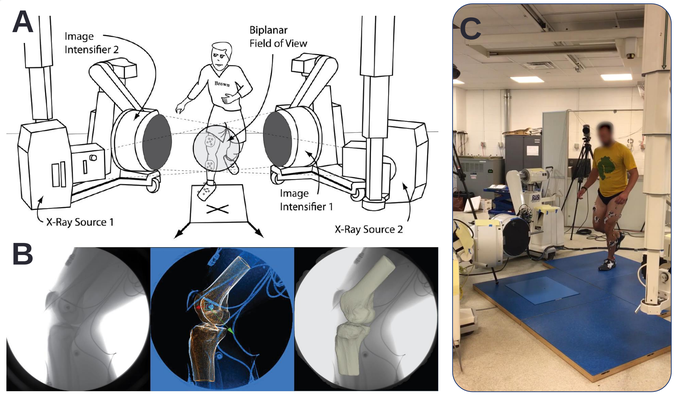


***Figure 1.*** *BVR uses two x-ray sources and image intensifiers **(A)** to capture bony motion. Subject-specific bone models are then matched to their underlying x-ray alignment in each x-ray view to reconstruct 3D kinematics **(B)**. After providing written informed consent, subjects performed a 1-leg hop activity while the landing was recorded **(C)**.*

**1° Outcome variables:**

- Anterior tibial position at ground contact
- Anterior tibial position as a function of flexion angle

**2° Outcome variables:**

- Knee flexion angle at ground contact
- Flexion and tibial internal/external (IE) range of motion

**Statistical Approach:** Generalized estimating equations with linear contrasts were used to test for differences between ACLR surgical and contralateral limbs, and between ACLR and controls. The Holm test was used to adjust for multiple comparisons while maintaining an alpha of 0.05.

## Results

**Mean anterior tibial position and flexion angle were not different between groups (Fig 2. A-B), but for the same flexion angle ACLR patients landed with their surgical and contralateral limb tibias positioned more anteriorly than controls by 10.3mm [1.7-19.0mm] and 7.5mm [1.8-13.2mm] (Fig 2. C-E).**

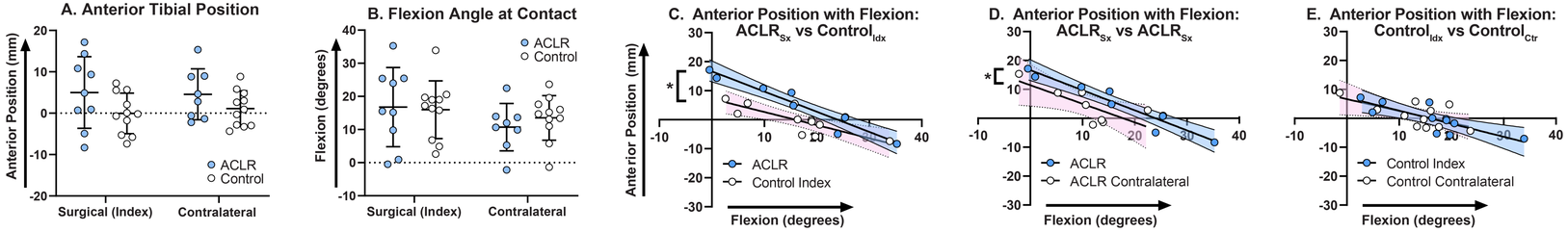


***Figure 2.*** *ACLR data are shown in blue; Control data are shown in open white. Blue (ACLR) and pink (Control) shaded regions in **(C-E)** show the 95% confidence interval of the regression. "*" in **(C&D)** indicate a significantly different y-intercept between groups. "Sx"=surgical limb. "Idx"=index limb. "Ctr"=contralateral limb.*

ACLR patients also had reduced internal tibial range of motion (not shown), while controls were symmetrical in all measures (e.g., Fig 2.E).

## Conclusion & Clinical Implications

- ACLR patient knee alignment may represent a predisposition to (re)injury, and/or contralateral limb motion may be the result of neuromuscular system adaptation.
- The contralateral limb should not be considered equivalent to a healthy control in a research setting and caution is warranted in using it as a functional target, particularly in the later stages of rehabilitation.

## Acknowledgements & References

This work was supported by NIH NIAMS K99/R00-AR069004; R01-AR047910; R01-AR074973; NIGMS P30-GM122732; and the Lucy Lippitt Endowment.

1. Kim, SY et al. (2015) AJSM 43(10); 2. Webster, KE et al. (2014) AJSM 42(3); 3. Lohmander, LS et al. (2004) Arthritis Rheum 50(10); 4. Davies, GJ et al. (2017) Curr Rev Musculoskeletal Med 10(3); 5. Akelman, MR et al. (2016) AJSM 44(7); 6. Miranda, DL et al. (2011) J Biomech Eng 133(12).

# New Potential to Restore Neuromuscular Function after ACL Injury: An RIH Injury COBRE Project Proposal

[1] Beveridge, JE, Fleming, BC. RIH Department of Orthopaedics Bioengineering Lab

jillian_beveridge@brown.edu

UNIVERSITY ORTHOPEDICS
INJURY CONTROL COBRE
Lifespan Orthopedics Institute
Rhode Island Hospital • The Miriam Hospital
Newport Hospital
*Delivering health with care®*

## Introduction

- Anterior cruciate ligament reconstruction (ACLR) using a tendon taken from elsewhere in the body is the current standard-of-care treatment for ACL tear (Fig 1. A).
- ACLR restores gross knee function to within 10% of contralateral limb values,[1] but neuromuscular function and joint motion remain distinctly different from uninjured persons,[2,3] potentially contributing to re-injury risk.[4]
- Bridge-enhanced ACL restoration (BEAR) is a new procedure that restores native ACL anatomy (Fig 1. B),[5] with BEAR patients regaining lower limb strength more fully and reporting better quality of life and superior return to sport metrics.[6]

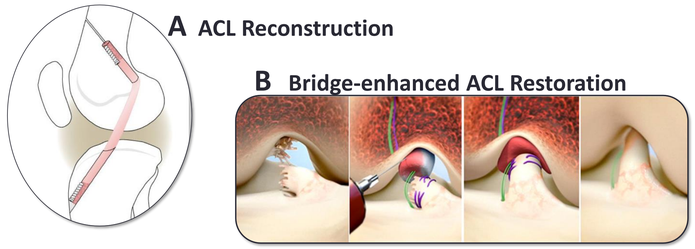


***Fig 1.** Competing ACL surgical techniques.*

***Our over-arching hypothesis is that BEAR surgery preserves neuromuscular activation patterns that, in turn, promote normal knee motion and superior patient-reported outcomes***

## Proposed Aims

**Aim 1:** Apply our machine learning approach to classify neuromuscular activity patterns within ACLR, BEAR, and healthy Control groups.

**Aim 2:** Compare ACLR, BEAR, and Control subject knee motion during a hop landing.

**Aim 3:** Examine the agreement between functional measures (neuromuscular activity, knee motion) and patient-reported outcomes.

## Methods

**Subjects:** 26 subjects from the BEAR-MOON Trial (NCT03776162) will be recruited at their 2-year follow-up: 13 BEAR and 13 ACLR. 13 Control subjects will be recruited and will be age- and sex- matched proportionally to the overarching BEAR Trial enrollment.

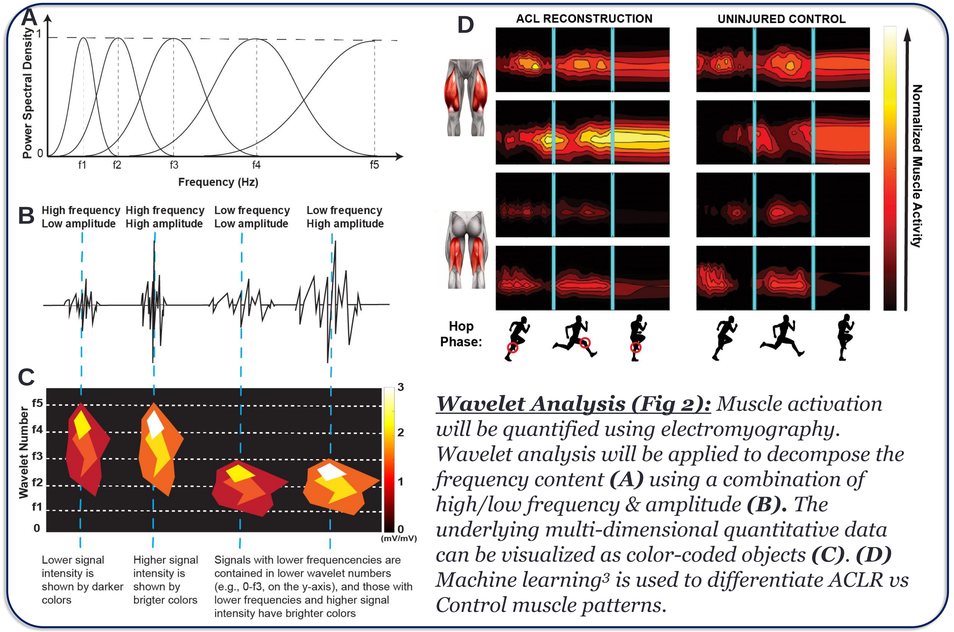


***Wavelet Analysis (Fig 2):** Muscle activation will be quantified using electromyography. Wavelet analysis will be applied to decompose the frequency content **(A)** using a combination of high/low frequency & amplitude **(B).** The underlying multi-dimensional quantitative data can be visualized as color-coded objects **(C)**. **(D)** Machine learning[3] is used to differentiate ACLR vs Control muscle patterns.*

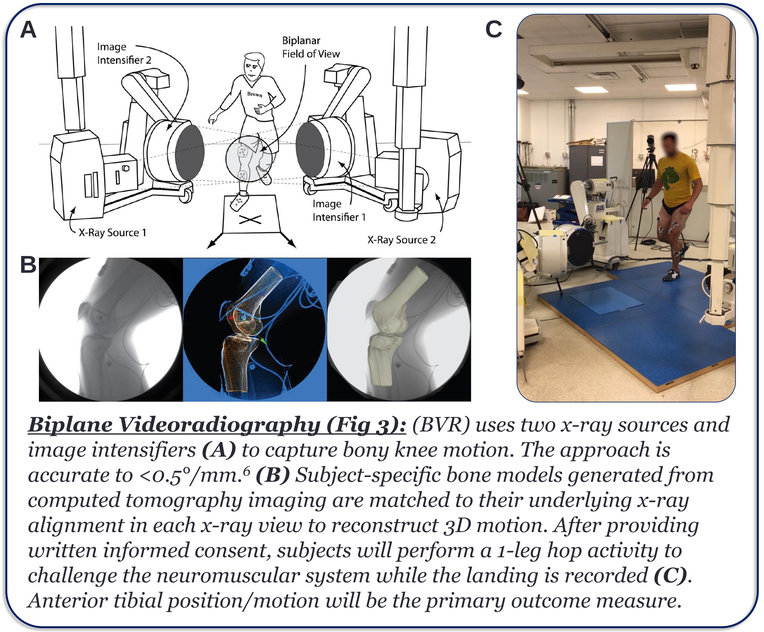


***Biplane Videoradiography (Fig 3):** (BVR) uses two x-ray sources and image intensifiers **(A)** to capture bony knee motion. The approach is accurate to <0.5°/mm.[6] **(B)** Subject-specific bone models generated from computed tomography imaging are matched to their underlying x-ray alignment in each x-ray view to reconstruct 3D motion. After providing written informed consent, subjects will perform a 1-leg hop activity to challenge the neuromuscular system while the landing is recorded **(C)**. Anterior tibial position/motion will be the primary outcome measure.*

**Patient-reported Outcomes (PROMs) (Aim 3):** The Sport and Recreation subscale from the Knee Injury and Osteoarthritis Outcome (KOOS) questionnaire is the primary outcome; secondary outcome is KOOS Quality of Life subscale; PROMs from additional questionnaires will be explored.

**Statistical Approach:** **Aim 1.** A kNN machine learning algorithm will differentiate muscle patterns between groups. **Aim 2.** Generalized linear models (GLM) with linear contrasts corrected with Holm tests will test for differences in anterior tibial position between groups. **Aim 3.** A support vector machine with a normalized vector magnitude (length) 0-1 will quantify neuromuscular abnormality with longer vectors indicating greater abnormality. GLMs with binomial distribution and log link function will test for relationships between neuromuscular/motion function normality and PROMs.

## Expected Outcomes & Clinical Implications

- We believe restoring the native ligament anatomy with BEAR will promote normal post-surgical neuromuscular function and joint motion, in turn leading to better quality of life satisfaction and a lower risk of reinjury that can be followed longitudinally.
- The wavelet-based metrics of neuromuscular function could be applied clinically to optimize rehabilitation, a new effort that is well suited to the Injury COBRE RPP Core.

## Acknowledgements & References

This work was supported by NIH NIGMS P20-GM1239664 (RIH Injury Control COBRE), NIAMS K99/R00-AR069004; R01-AR047910; R01-AR074973; and the Lucy Lippitt Endowment.

1. Akelman, MR et al. (2016) AJSM 44(7); 2. Beveridge, JE at al. (2020) Trans ORS; 3. Zandiyeh, P et al. (2022) J Biomech 33; 4. Webster, KE et al. (2014) AJSM 42(3); 5. Murray, MM et al. (2013) AJSM 41(8); 6. Murray MM et al. (2020) AJSM 48(6); 7. Miranda, DL et al. (2011) J Biomech Eng 133(12).

# Approach for Evaluating Cartilage Thickness Based on Patient Geometry

Crystal J. Murray,[1,2] Janine Molino,[1,2] Braden C. Fleming,[1,2] Jillian E. Beveridge[1,2]
[1]Rhode Island Hospital, Providence, RI, [2]Brown University, Providence, RI

## Introduction

Anterior cruciate ligament reconstruction (ACLR) does not reduce the risk of post-traumatic osteoarthritis, a degenerative condition characterized by early cartilage swelling followed by progressive cartilage loss.

We developed an approach to quantify sub-regional medial femoral condyle (MFC) cartilage thickness that could be scaled to account for differences in knee size.

## Hypotheses

We hypothesized that:

1) MFC cartilage thickness in ACLR patients (10-15 years post-surgery) would be thinner than uninjured controls.

2) MFC cartilage in uninjured female controls would be thinner than in uninjured male controls.

## Methods

IRB-Approved Study

**Subjects**: 9 ACLR patients (4M/5F; 10-15 years post-surgery; mean age 34±10.5 years) and 12 uninjured controls (7M/5F; no history of knee injury; mean age 38±7.4 years).

**Data:** Tibiofemoral cartilage segmented from magnetic resonance (MR) images (FLASH sequence). Femoral bony geometry segmented from computerized tomography (CT) scans.

**Analysis:** Segmented images were used to generate 3D models and orient each patient's cartilage into a common coordinate system. Cartilage thickness was mapped between subchondral bone and cartilage surfaces. Based on the width and curvature of the condylar cartilage, 24 proportionally distributed MFC sub-regions were generated on the cartilage.

**Statistics:** Mixed linear models were used to test the study hypotheses. Pairwise comparisons were conducted via orthogonal contrasts. The Holm test was used to maintain a two-tailed familywise alpha at 0.05.

## Results

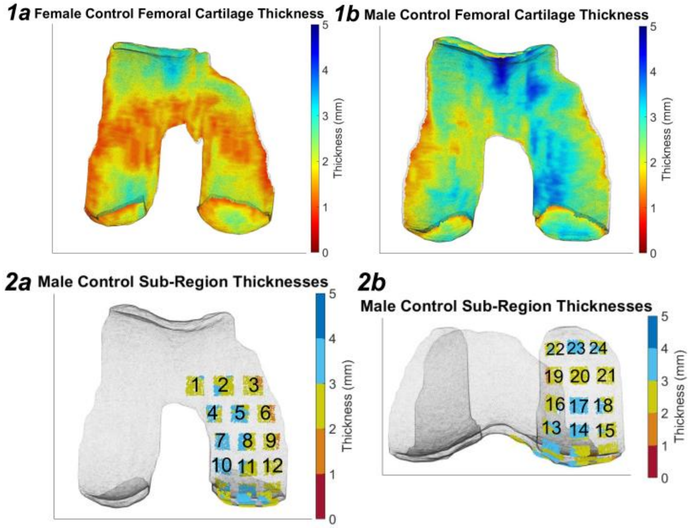


Figure 1 (a-b): Color maps of cartilage thickness.

Figure 2 (a-b): Indexed MFC cartilage.

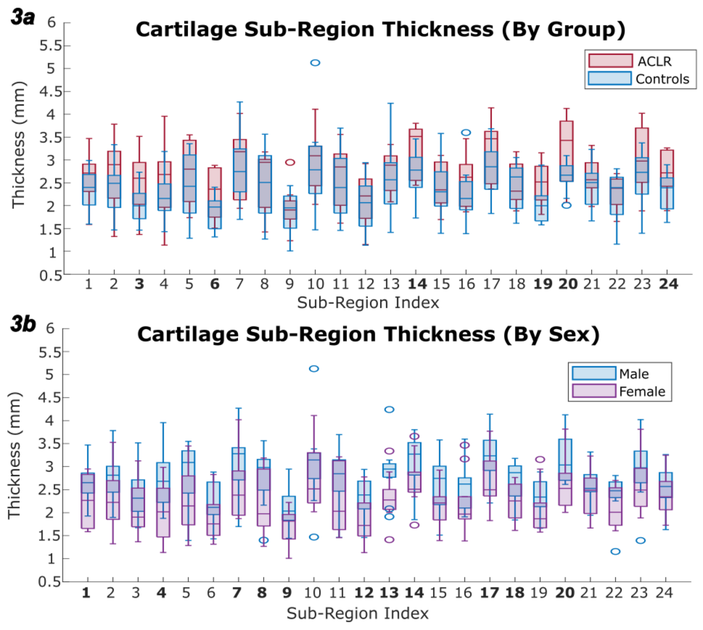


Figure 3 (a-b): Box plots of sub-regional analysis.

Numbered sub-regions on the x-axis correspond to the mapped locations (in Figure 2), bolded text indicates significant differences between Group/Sex before adjusting for multiple comparisons.

## Results (continued)

1) ACLR patients tended (p=0.056) to have thicker MFC cartilage 10-15 years post-surgery.

- A significant interaction between group and sub-region was detected (p<0.0001)

2) Cartilage thickness was not different (p=0.069) between female and male uninjured controls. However:

- A pooled analysis of both ACLR patients and controls showed that females had significantly (p=0.004) thinner MFC cartilage.
- A significant interaction between sex and location was detected in both the control-only (p=0.003) and pooled analyses (p<0.0001).

## Discussion

**Our results highlighted a trend towards ACLR patients having thicker MFC cartilage than uninjured controls.**

- **This suggests that 10+ years after ACLR surgery, these patients present with cartilage swelling rather than thinning.**

Trends in our results were consistent with the literature describing females having thinner cartilage than males [1].

The sub-regional approach to quantify cartilage thickness differences revealed potentially clinically relevant cartilage thickening that likely would have been overshadowed if expressed as a mean of the entire surface.

[1] Otterness, I. G., et al. Osteoarthritis Cartilage (2007)

## Clinical Relevance

Coupled with AI-based algorithms for automatic cartilage model generation, the approach could be applied to larger cohorts to monitor cartilage changes earlier in the disease trajectory when interventions may be more effective.

## Acknowledgements

NIH NIAMS K99/R00-AR069004; R01-AR047910; R01-AR074973; NIGMS P30-GM122732; Lucy Lippitt Endowment

# Approach for Evaluating Cartilage Thickness Based on Patient Geometry

Crystal J. Murray,[1,2] Janine Molino,[1,2] Braden C. Fleming,[1,2] Jillian E. Beveridge[1,2]
[1]Rhode Island Hospital, Providence, RI, [2]Brown University, Providence, RI

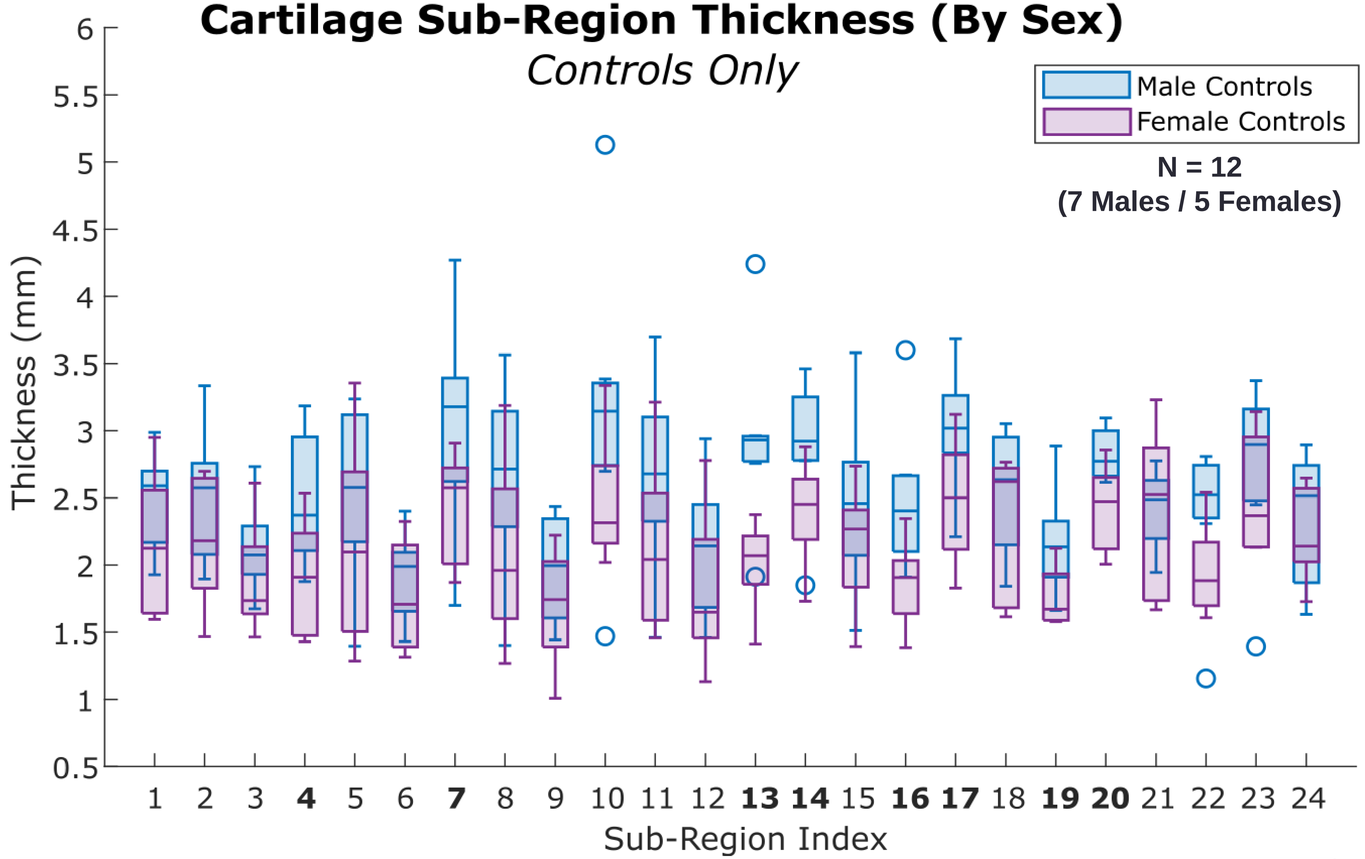


## Description

Box plot of sub-regional analysis demonstrating significant MFC cartilage differences between male and female control participants. Numbered sub-regions on the x-axis correspond to the mapped locations (on the right),. Bolded text indicates significant differences between male and female participants before adjusting for multiple comparisons.

In this analysis of controls, cartilage thickness was not different (p=0.069) between males and females (2.13mm, 95% CI=1.83-2.43 versus 2.54mm, 95% CI=2.22-2.87). This is a **-16% mean difference in female cartilage thickness.**

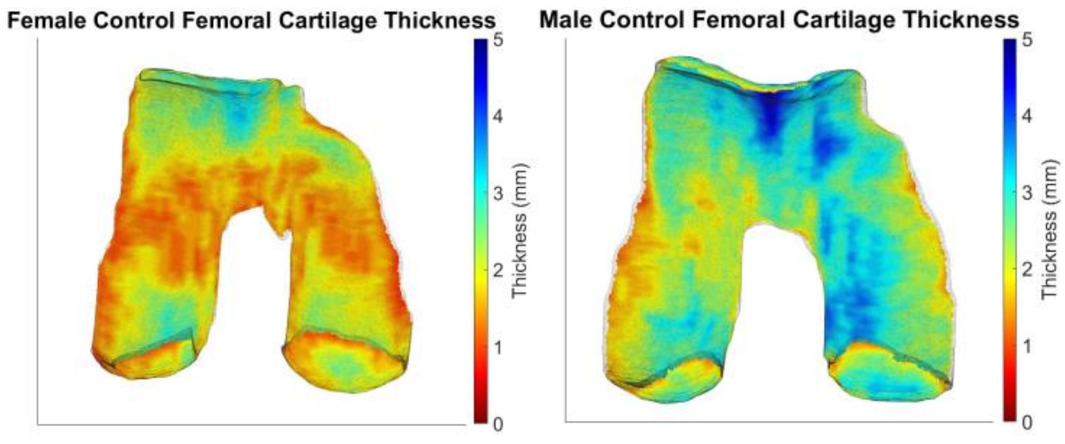


Color maps of cartilage thickness for representative female (left) and male (right) control subjects.

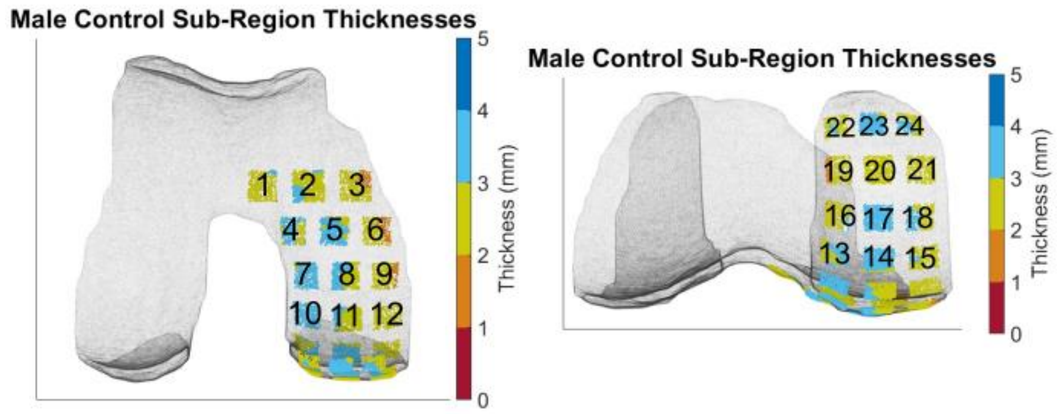


Indexed MFC sub-regions with underlying cartilage thickness corresponding to the colormaps above.

Main Poster

# Approach for Evaluating Cartilage Thickness Based on Patient Geometry

Crystal J. Murray,[1,2] Janine Molino,[1,2] Braden C. Fleming,[1,2] Jillian E. Beveridge[1,2]
[1]Rhode Island Hospital, Providence, RI, [2]Brown University, Providence, RI

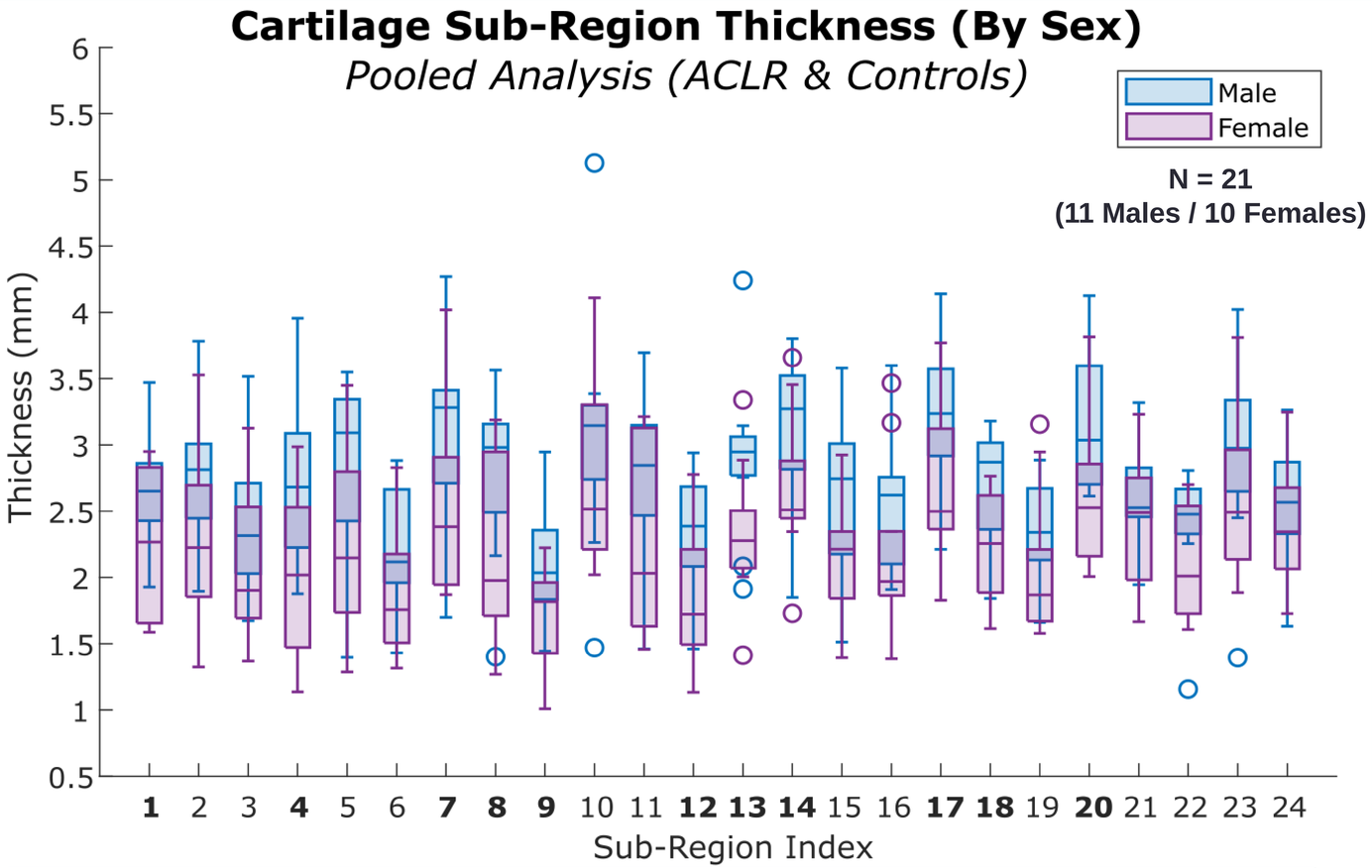


## Description

Box plot of sub-regional analysis demonstrating significant MFC cartilage differences between male and female participants (independent of ACLR or control). Numbered sub-regions on the x-axis correspond to the mapped locations (on the right). Bolded text indicates significant differences between male and female participants before adjusting for multiple comparisons.

In this pooled analysis (of ACLR & control patients), females had significantly (p=0.004) *thinner* MFC cartilage than males(2.26mm, 95% confidence interval (CI)=1.99-2.54 versus 2.76mm, 95% CI = 2.57-2.95) This is a **-18% mean difference in female cartilage thickness**.

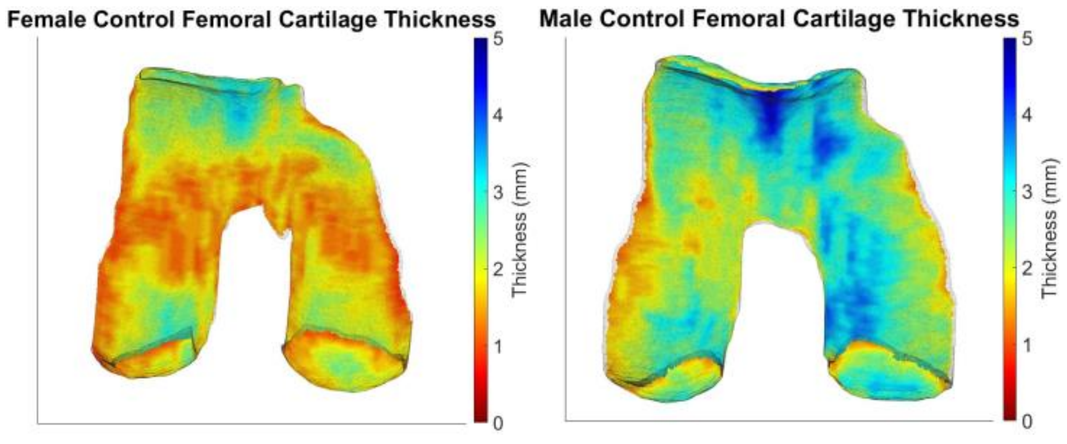


Color maps of cartilage thickness for representative female (left) and male (right) control subjects.

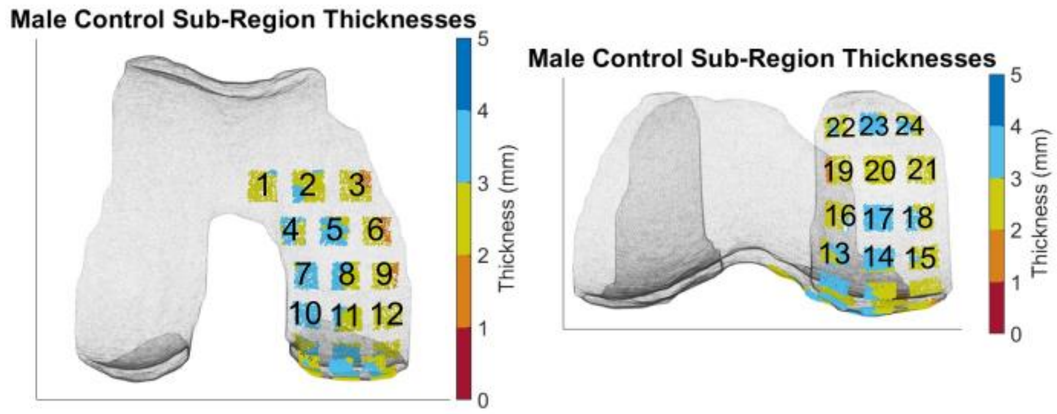


Indexed MFC sub-regions with underlying cartilage thickness corresponding to the colormaps above.

Main Poster

# Approach for Evaluating Cartilage Thickness Based on Patient Geometry

Crystal J. Murray,[1,2] Janine Molino,[1,2] Braden C. Fleming,[1,2] Jillian E. Beveridge[1,2]
[1]Rhode Island Hospital, Providence, RI, [2]Brown University, Providence, RI

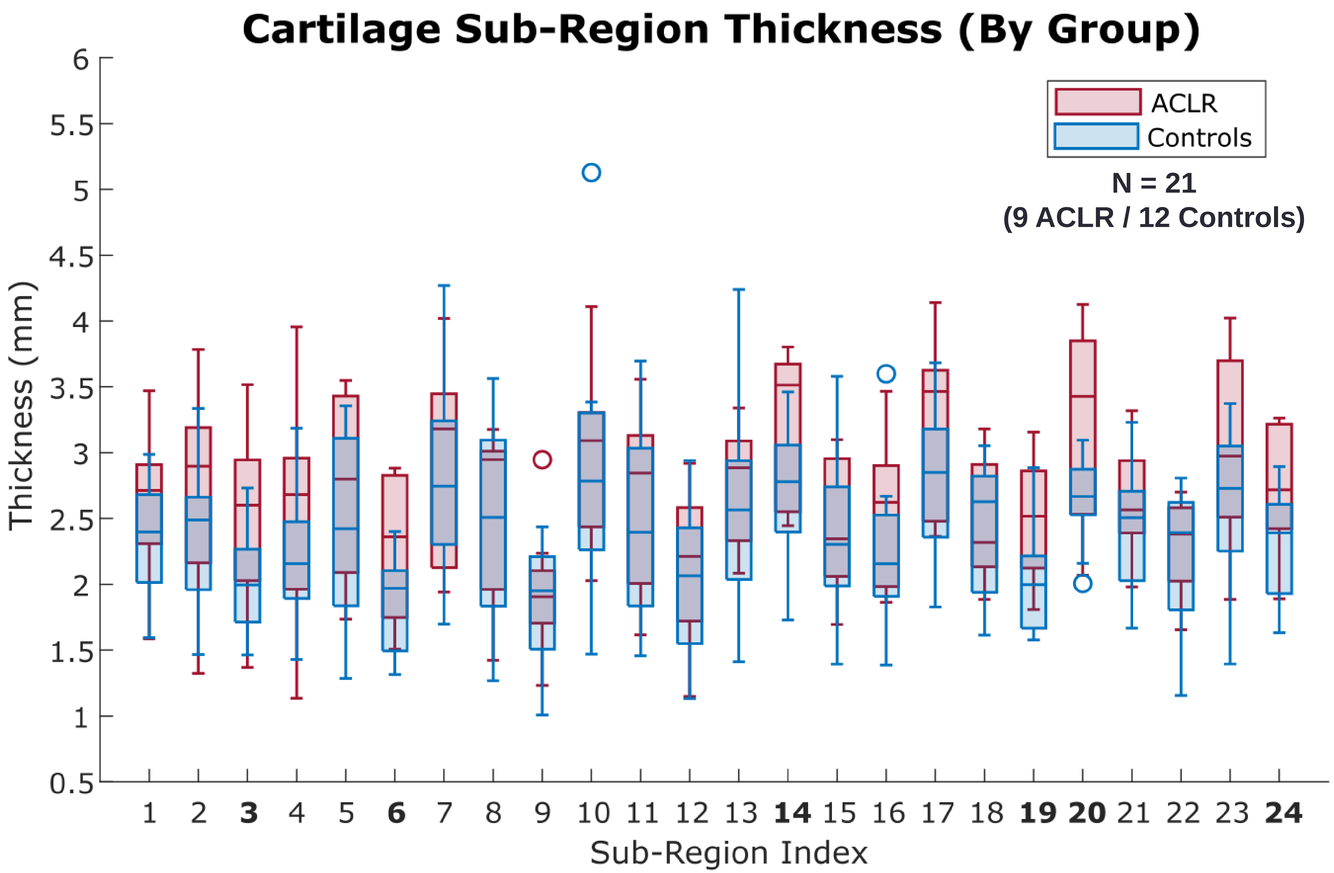


## Description

Box plot of sub-regional analysis demonstrating significant MFC cartilage thickening in ACLR subjects (independent of male or female). Numbered sub-regions on the x-axis correspond to the mapped locations (on the right). Bolded text indicates significant differences between ACLR and controls before adjusting for multiple comparisons.

ACLR patients tended (p=0.056) to have *thicker* MFC cartilage than uninjured controls (2.68mm, 95% CI=2.42-2.95 versus 2.34mm, 95% CI=2.10-2.57). This is a **+13% mean difference in ACLR cartilage thickness.**

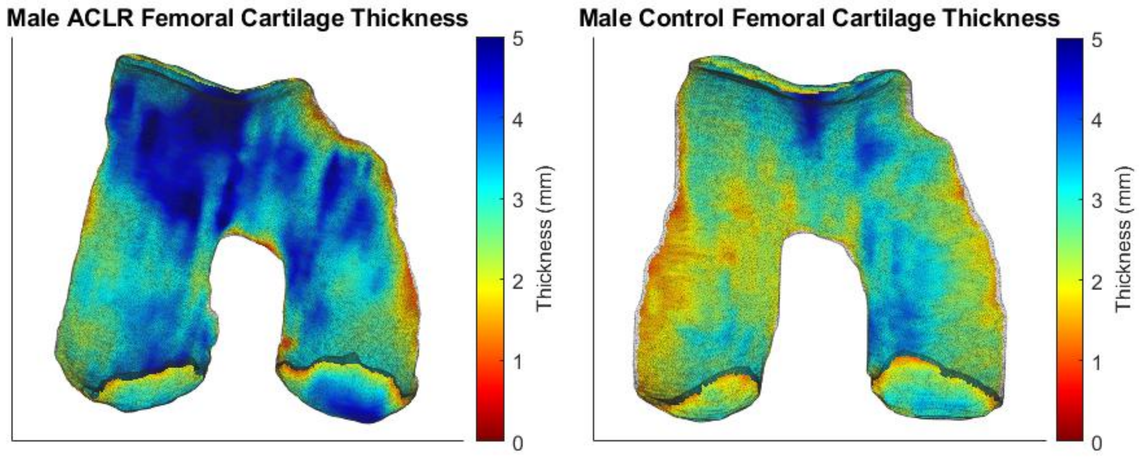


Color maps of cartilage thickness for representative male ACLR patient (left) and male uninjured control(right).

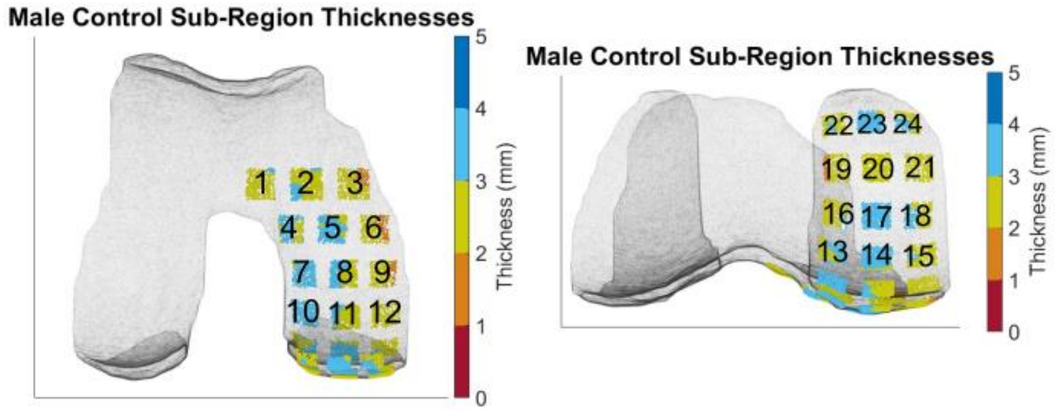


Indexed MFC sub-regions with underlying cartilage thickness corresponding to the colormaps above.

Main Poster

# Accuracy and Precision of Markerless Bone Tracking Relative to the Gold-Standard Marker-Based Method

John Holtgrewe[1], Braden C. Fleming[1], Jillian E. Beveridge[1]

[1]Brown University and Rhode Island Hospital, Providence, RI

## Background and Aim

- Biplane video radiography (BVR) is used to quantify 3D skeletal joint motion using either gold-standard marker-based, or the more clinically applicable, markerless tracking.
- Marker-based tracking is accurate to ~0.25°/mm,[1] but requires surgically implanting metal beads.
- Markerless tracking depends on the bone shape and is dependent on biplane system geometry and bone-soft tissue image contrast.
- Knowledge of accuracy and precision of a BVR geometry optimized for knee motion recording will be important for interpreting expected clinical differences in joint motion between healthy and injured persons.

**Aim: To quantify accuracy and precision of markerless tracking for a hop landing task using beaded data as the gold-standard reference.**

## Methods

- 14 tantalum beads were implanted in cadaveric knee specimen; 6 in the femur and 8 in the tibia
- Femur and tibia models generated from computed tomography (CT) scans
- Specimen was frozen and moved through a calibrated biplane system field of view, simulating a hop landing motion
- Marker-based tracking was conducted by digitizing and tracking the displacement of the beads in the x-ray videos using specialized software (XMALab)[2]

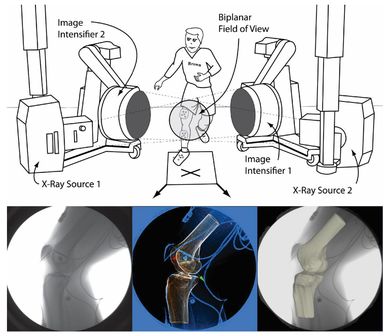


*Figure 1. (Top) BVR setup diagram with human subject (Bottom Left to Right) X-ray video frame, aligning models with radiographs using Autoscoper, visualizing bone motion using 3D models*

- X-ray videos and CTs were then processed to remove the spatial information associated with the beads, then markerless tracking was conducted by matching the markerless bone models to the x-ray videos using 2D-3D registration software (Autoscoper, Brown University)[3]

## Methods cont.

- Analyses performed for each trial using the first 38 frames where both femur and tibia were visible in the field of view
- 3D knee motion calculated for both tracking methods, expressed as 6 degrees of freedom (6DOF) — 3 rotations and 3 translations

## Results

- Mean absolute differences in flexion/extension (FE), ab/adduction (AA), and internal/external (IE) rotation were 0.19±0.24°, 0.36±0.20°, and 0.64±0.55°
- Translational differences in medial/lateral (ML), anterior/posterior (AP), and inferior/superior (IS) directions were 1.62±0.34mm, 0.20±0.26mm, and 0.14±0.09 mm
- Bland-Altman analyses revealed biases of -0.07°, 0.24°, and 0.58° in FE, AA, and IE rotation, respectively; biases in the ML, AP, and IS translational DOFs were -1.60mm, 0.19mm, and -0.12mm, respectively
- Limits of agreement (1.96xSD) of 0.59°, 0.66°, 1.2° for FE, AA, and IE rotation, respectively; limits of agreement for ML, AP, and IS translation were 0.66mm, 0.51mm, and 0.23mm, respectively

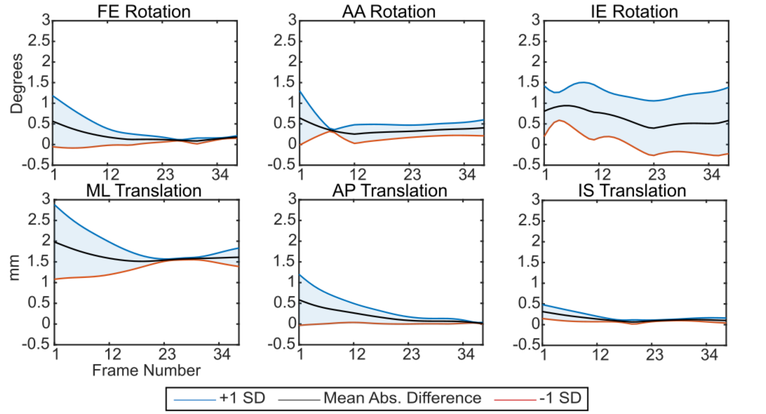


*Figure 2. Mean absolute difference between tracking approaches for each DOF*

## Results cont.

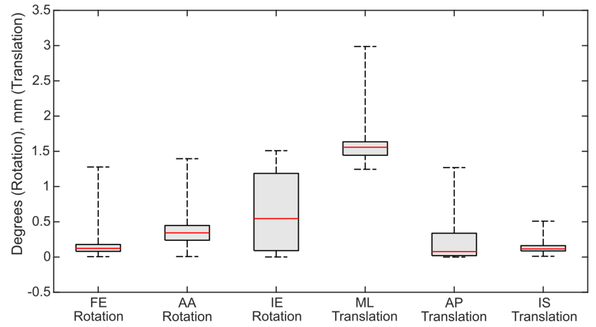


*Figure 3. Absolute difference between tracking methods by DOF*

## Discussion

- ML translation was the least accurate DOF; likely the result of ML translations occurring in the plane normal to image intensifier (i.e., out-of-plane motion)
- System geometry was optimized to capture in-plane AP translation, so ML translation inaccuracies not unexpected
- We have previously reported that ACL reconstructed patients land with their tibia anteriorly translated by up to 7.5mm during a hop-landing compared to matched uninjured patients[3]
- 7.5mm is more than an order of magnitude greater than the level of imprecision quantified in the AP DOF, giving us high confidence that our BVR configuration and post-processing approach are sensitive to meaningful changes in the population of interest

## Conclusions

The accuracy, precision, and bias of 3D joint motion obtained from our hop landing biplane videography system configuration is dependent on the DOF of interest but are an order of magnitude superior to the precision of conventional motion capture approaches.[4]

## Acknowledgements & References

This project was supported by the NIH/NIAMS (K99/R00-AR069004, R01-AR047910, R01-AR074973), NIGMS (P30-GM122732, P20-GM139664) and the Lucy Lippitt Endowment.

1. Miranda, D. et al. J Biomech (133), 2011. 2. Knörlein, B. et al. J Exp Biol (219), 2016. 3. Beveridge, JE. Et al. Trans ORS, 2020. 4. Miranda, D. et al. J Biomech (46). 2013.

# A ROBOT-ACTUATED IN VITRO TESTING APPROACH FOR QUANTIFYING PASSIVE RANGE OF MOTION IN THE THUMB CMC JOINT

JM Kalshoven[1]*, R Badida[1], AM Morton[1], DC Moore[1], JJ Crisco[1]
[1]Department of Orthopaedics, Warren Alpert Medical School of Brown University and Rhode Island Hospital, Providence RI
*corresponding author email: josephine@brown.edu

## Introduction

Studies have found that active and passive ranges of motion (ROM) are reduced in thumb carpometacarpal (CMC) joint osteoarthritis (OA), yet the underlying causes remain unclear [1]. Osteophyte growth and ligament property changes associated with progressive disease have been hypothesized to affect CMC ROM, yet no study has confirmed a causal relationship. An *in vitro* ROM assessment would eliminate neuromuscular influence and allow for prescribed, directional load application, shedding light on inherent stabilizing structures.

The aim of this work was to develop an approach to determine the multi-directional biomechanics of the CMC joint *in vitro* and demonstrate its implementation in six pilot specimens.

## Methods

The proposed approach builds a biomechanical picture of the CMC joint ROM from 32 tests of first metacarpal (MC1) motion with respect to the trapezium (TPM) recorded in 6 degrees of freedom (DOF) with a robotic testing system. Robotic motion of the CMC joint included:

- **Rotational ROM** in flexion (FL), extension (EX), abduction (AB), and adduction (AD), and in 20 coupled directions (15-degree increments of flexion-adduction, extension-abduction etc.)
  - $1^0$/s to a limit of 1.0 Nm resultant torque (RMS of 3 rotational DOF)
- **Translational ROM** in volar (V), dorsal (D), radial (R), ulnar (U), and in four combined directions
  - 1 mm/s to a limit of 30N resultant force (RMS of 2 translational DOF: volar/dorsal and radial/ulnar)

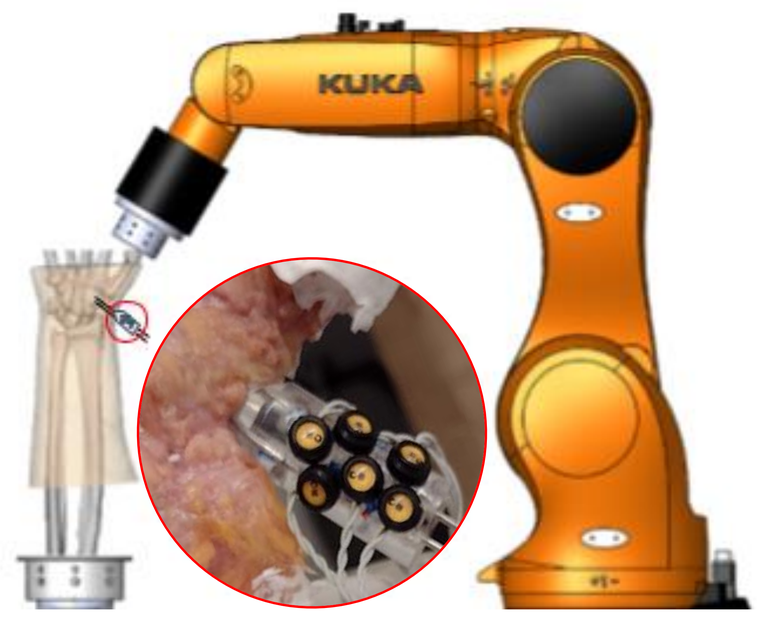


**Fig 1. Specimen mounted to robotic musculoskeletal simulation system.** Inset: Sensor for tracking TPM motion.

Six fresh-frozen human forearms (4M, 2F, 27-63 yrs.) were sectioned proximally at the midshaft of the radius/ulna. All bones distal to the carpus were removed, except for the first metacarpal (MC1) and the proximal head of the second metacarpal (MC2). The bone ends were potted for fixation to the robot (Figure 1).

A cluster of 6 infrared markers (NDI) was rigidly mounted via k-wires to the trapezium (TPM) to track the motion of the TPM (Figure 1). A CT scan of each specimen was acquired and segmented using established methods [2]. Bone surface meshes and fiducial point coordinates were exported. MC1 and TPM bone coordinate systems (CS) were computed based on directions of principal curvature of the articular surfaces[3] and, for the MC1, its proximal-distal inertial axis. CS were directed volarly (+x), proximally (+y), and radially (+z) (Figure 2).

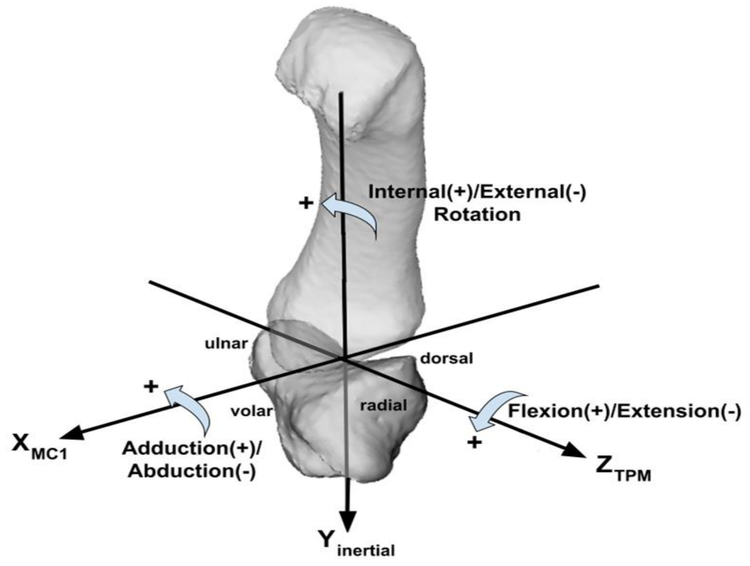


**Fig 2. CMC joint axes and rotations.**

All tests began from CMC joint neutral, defined as:
1) $0^0$ MC1 rotation in FL/EX/ AB/ AD;
2) 2 N proximal compression and 0 N in V/D/R/U joint forces;
3) 0 Nm torque in internal/external rotation (IR/ER).

For each test, force-displacement and torque-rotation curves were analyzed from 6 DOF kinematics and kinetics. Polar plots of ROM envelopes were generated from max ROM in each direction.

## Results

Data demonstrate ROM variability across individuals (Figure 3):

- Average rotational standard deviation (all directions)= $14^0$
  - Max Std Dev = $23.7^0$ in abduction-flexion
- Average translational standard deviation(all directions)= 3 mm
  - Max Std Dev = 4.7 mm in volar-ulnar translation
- The greatest rotational ROM was in the combined abduction-flexion region for 4/6 specimens
- Half of the specimens exhibited less translation in the dorsal and radial directions than the volar and ulnar directions

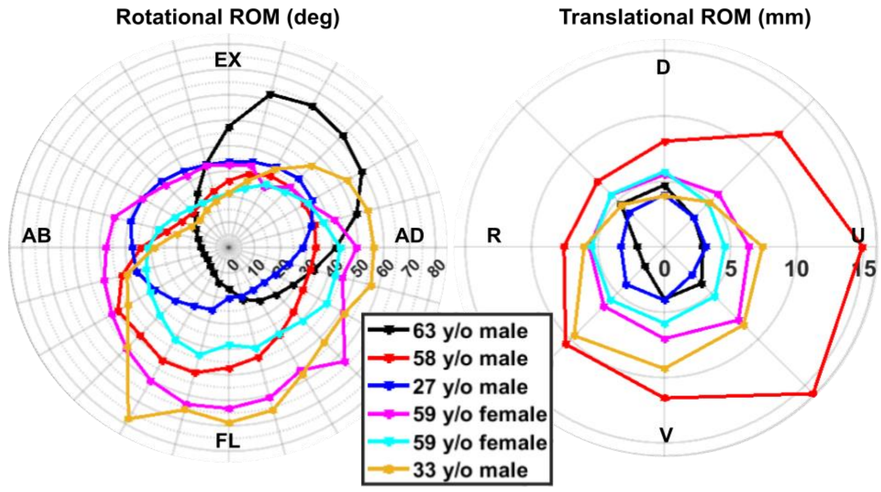


**Fig 3. ROM envelopes for all 6 specimens.**
**L: Rotational ROM** (°) in 24 directions at 1 Nm. EX-extension, AD-adduction, FL-flexion, AB-abduction.
**R: Translational ROM** (mm) in 8 directions at 30 N. D- dorsal, U-ulnar, V-volar, R-radial

## Discussion

Our work demonstrates the novel ability to isolate and determine the CMC joint ROM *in vitro* by manipulating the MC1 and accounting for TPM motion with an attached Sensor. The variability of CMC ROM across pilot specimens from a wide age range suggests substantial ROM variation throughout the population. Future analysis grouped by OA presence, age, or sex, may yield clearer patterns, as the oldest specimen (and the only one with documented hand OA) demonstrated a distinctly larger extension and smaller flexion ROM than other specimens. Patterns emerged in some specimens, such as maximal range of motion in flexion and flexion-coupled directions, which are most utilized for grips, and greatest stiffness in dorso-radial directions, which is consistent with stability for preventing dorso-radial subluxation of the joint under common grip forces.

Our varied results underscore the need for additional data and grouped analysis, as well as motivate future studies on ligament integrity and osteophyte volume as structural influences on ROM.

## Significance

These results demonstrate the feasibility of determining *in vitro* CMC biomechanics across a spectrum of joint conditions, such as OA degeneration. Such data would build a more-complete understanding of the interplay of pathology and joint integrity, which will inform our understanding of consequences of disease progression.

## References

1. Gehrmann, *J Hand Surg Am*, 2010.
2. Badida, *J Biomech Eng*, 2020.
3. Halilaj, *J Biomech*, 2013.

Lab Website

# Skin Motion Artifact of Radiopaque Bead Tracking Relative to Markerless Bone Tracking

QM Vaughan[1], AM Morton[2], T Hayda[2], JJ Crisco[1, 2]

[1]*Center for Biomedical Engineering and School of Engineering, Brown University, Providence, RI 02912, United States*

[2]*Department of Orthopedics, The Warren Alpert Medical School of Brown University and Rhode Island hospital, Providence, RI 02903, United States*

## Introduction

Biplanar videoradiography (BVR) is considered the gold standard when measuring dynamic *in vivo* joint kinematics because it enables the tracking of the skeletal structures rather than skin-based markers. It has been well established that skin-based markers when used to study the underlying skeletal kinematics are associated with soft tissue artifact (STA). Assessing the scope of STA in tracking skeletal joints is complex because the magnitude of the error is a function of many factors, including the specific joint, the type of task, the dynamics of the task, and the location of the markers. Our lab is focused on studying wrist function and the effects of pathologies and treatments, such as wrist arthroplasty.

**Thus, the focus of this study is to quantify STA of the wrist. We employed BVR as the gold-standard and bead displacement as a measure of STA.**

## Methods

Six subjects with no history of wrist or hand pathology were recruited for this project. All subjects were female (51-68 yrs). The individuals were instructed to complete 7 wrist motion tasks (1).

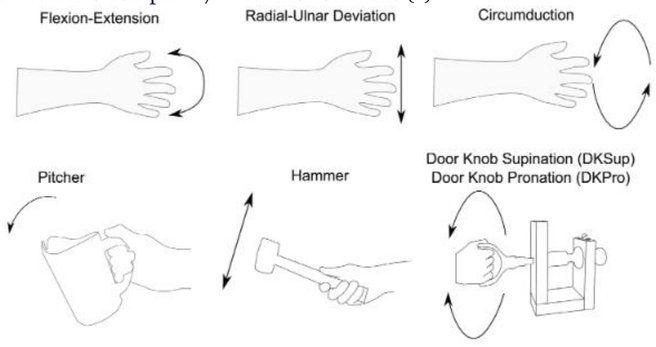


**Fig 1.** Seven hand and wrist motion tasks. (1)

Five radiopaque beads were placed on the dorsal surface of the hand to measure wrist motion. An average of 400 frames were recorded per task. The 3-D coordinates of the beads were tracked for all motion trials using XMALab.

Wrist motion for each task was defined as the motion of the third metacarpal (MC3) relative to the radius and was computed using BVR markerless bone tracking software (Autoscoper)(2). The accuracy to which the tracking software can detect the MC3 is validated by normalized cross-correlation (NCC).

STA was defined as the displacement of the average of the beads relative to a neutral pose and reported as a function of wrist motion within each task. Descriptive statistics were used to describe STA.

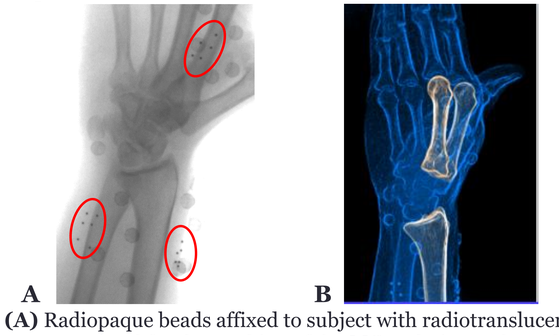


**Fig 2. (A)** Radiopaque beads affixed to subject with radiotranslucent tape. **(B)** Autoscoper visual for the tracking of the MC3 relative to the radius. (2)

## Results

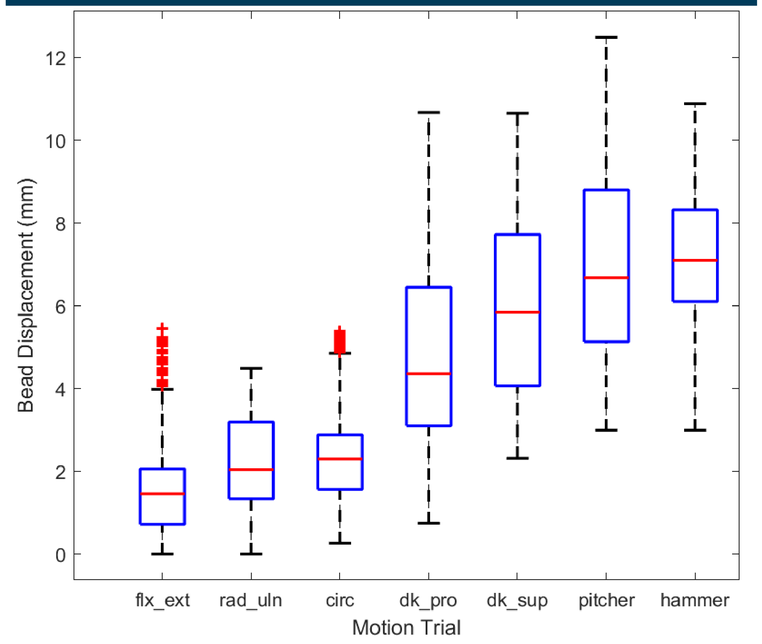


**Fig 3.** Boxplot of the magnitude of average bead displacement, defined as a measure of STA, for all subjects across every motion trial

- Pitcher pouring motion task had the greatest amount of bead displacement (~12.5 mm).
- Radial ulnar wrist motion yielded the smallest amount of bead displacement (~4.5 mm).
- Grasping motion tasks (dk_pro, dk_sup, pitcher, hammer) had a larger average of bead displacement (~11.2 mm) compared to open hand tasks (~5 mm).
- Circumduction motion task had the greatest number of outliers meaning the data portrayed a large range of bead displacement across subjects.

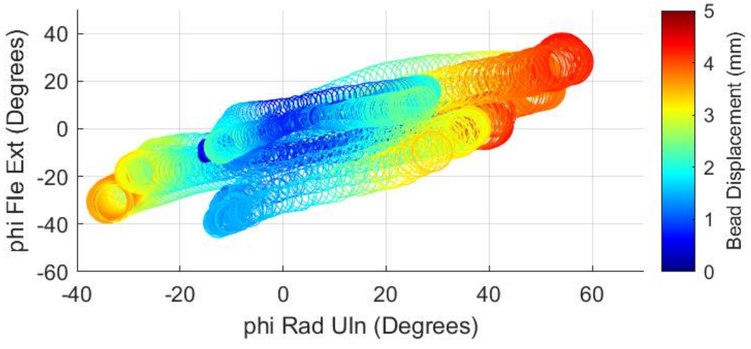


**Fig 4.** Degree of rotation (phi) for radial-ulnar and flexion-extension wrist motion of all subjects for the radial-ulnar deviation motion trial

- At maximum degree of ulnar deviation, subjects experienced maximum degree of flexion.
- Average bead displacement is reported in color bar format with maximum bead displacement (~5 mm) occurring at peak ulnar deviation and flexion.

## Discussion

- Grasping tasks yielded a higher average in bead displacement compared to open hand motion tasks due to the added stretch of the skin when holding an object.
- Subjects displayed wrist motion combinations for all motion trials resulting in an unexpectedly large range of degree of rotation across subjects.
- Large ranges of data for bead displacement and degree of rotation measurements indicates that the motion task was not uniformly performed by all subjects.

**Limitations**:

- Imprecise bone detection in radiographic images when using markerless bone tracking software (Autoscoper) causes inaccuracy in eliminating underlying bone motion to calculate STA.
- Misinterpretation of explained motion tasks across subjects causing inconsistencies in the start and end positions of the subject per trial and in calculating full degree of rotation.

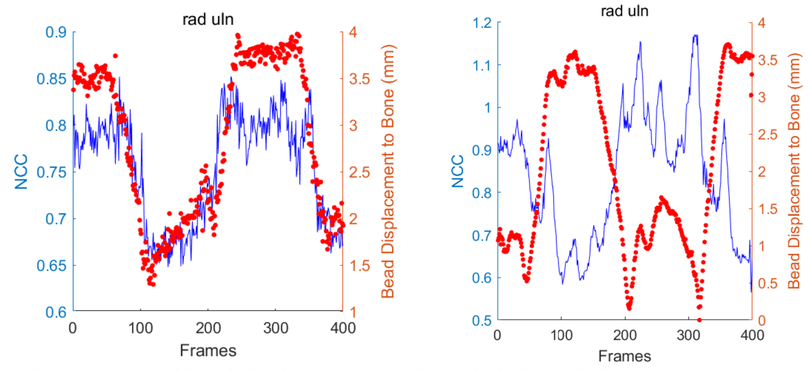


**Fig 6.** NCC and bead displacement for the radial ulnar deviation motion trial for two individual subjects.

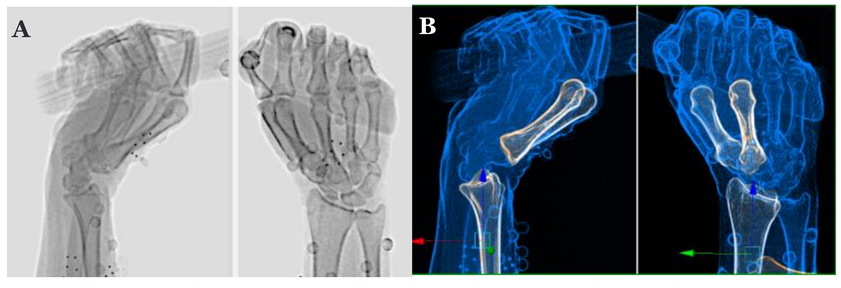


**Fig 7. (A)** Radiopaque bead locations relative to underlying bone. **(B)** Autoscoper bone detection for hammering task

## References

1. McHugh, B. et al., *Optical Motion Capture Accuracy is Task-Dependent in Assessing Wrist Motion,* 2021.
2. Akhbari, B. et al., *Biplanar Videoradiography to Study the Wrist and Distal Radioulnar Joints,* 2021.

## Acknowledgements

This research is supported in part by funding from NIH-NIGMS R25GM083270

# Post-Surgical Metal Wear Particle Artifact Correction in Magnetic Resonance Imaging by Deep Neural Networks

Dominique A. Barnes,[1,2] Jillian Green,[1,2] Connor Uzzo,[1,2] Ata M. Kiapour,[3] Martha M. Murray,[3] Sean W. Flannery, [1,2] Braden C. Fleming [1,2]
[1]Brown University, Providence, RI, [2]Rhode Island Hospital, Providence, RI, [3]Boston Children's Hospital, Boston, MA

## INTRODUCTION

- Anterior cruciate ligament (ACL) surgery generates metal wear particles in the joint space [1]
  - The particles can sometimes obstruct MR images of the ACL and surrounding tissues [1]
- Primary Goal: Train a deep learning model to correct magnetic susceptibility artifacts observed post-ACL surgery MR images
  - The goal of image correcting models are to identify artifacts in an MR image and correct pixel values by removing the artifact and filling the missing region based on the background information [2]
- Artifacts were generated to train each deep learning models and determine the optimal model to use
- Real artifacts were then used to test the models' correcting ability

## HYPOTHESIS

- The signal intensity (SI) obtained from the deep learning corrected artifact regions would not be significantly different from ground truth

## METHODS

### Data Collection

- The dataset included 120 patients who underwent ACL surgery
- MR images were collected from Constructive Interference in Steady State (CISS) scans acquisition matrix with voxel size 0.365mm x 0.365mm x 1.5mm
  - FA=35° ; TR=12.78ms; TE=6.39ms; FOV=140mm; 384 x 384
- MR images of the patients' intact ACL without metallic susceptibility artifacts were used in the dataset
- Real artifacts were segmented and overlaid onto the images used in the dataset (Figure 1)
- The MR image without the artifact overlaid were set as to validate the models used in this study

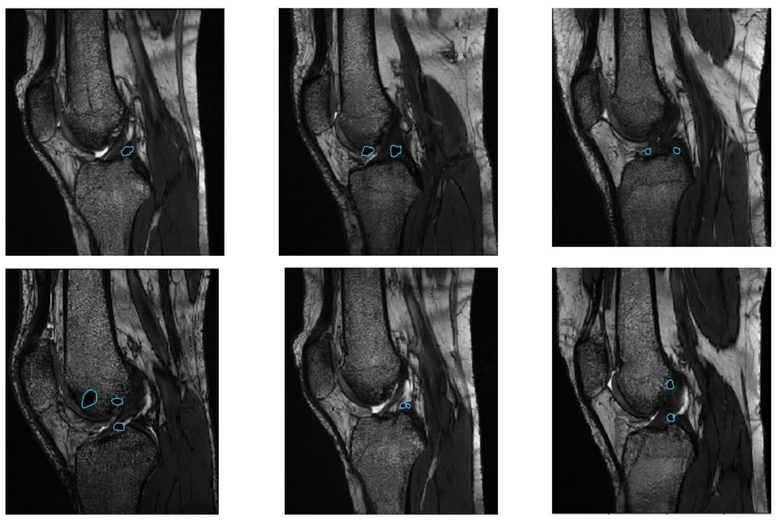

Figure 1. MR Images with real artifacts overlaid

## METHODS

### Models and Parameters

- Five models were evaluated:
  1. Shallow Dense network
  2. Deep Dense network
  3. Convolutional Neural Network (CNN)
  4. Composite model of Shallow-Dense network and the CNN
  5. Generative Adversarial Network (GAN)
- Models were constructed in TensorFlow 2.1.0 with Kera API
- The training was performed on the Google Cloud Platform
  - Virtual machine configuration of an n1-standard-8 CPU cluster and an NVIDIA T4
- Data split: 80% train (n=1376), 10% validation (n=172), and 10% test (n=172)
  - Test and train data are images that contain artifacts

### Real Artifact Segmentation

- Artifacts were segmented from MR images using the Materialise Mimics software
- Each slice of the MR image was assigned a label, feature number, and mask
- The feature numbers are the signal intensities belonging to the artifact (Figure 2)

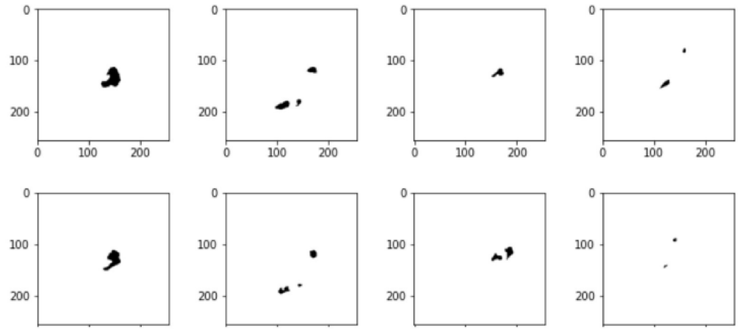

Figure 2. Real artifacts from MR Images

## RESULTS

### Visualizing Corrections

- A side-by-side comparison was done to visualize how well each model corrected an MR image (Figure 3)
- The Deep Dense model corrected the artifact region and included great image detail
- The CNN model was unable to correct the artifact region but enhanced image detail

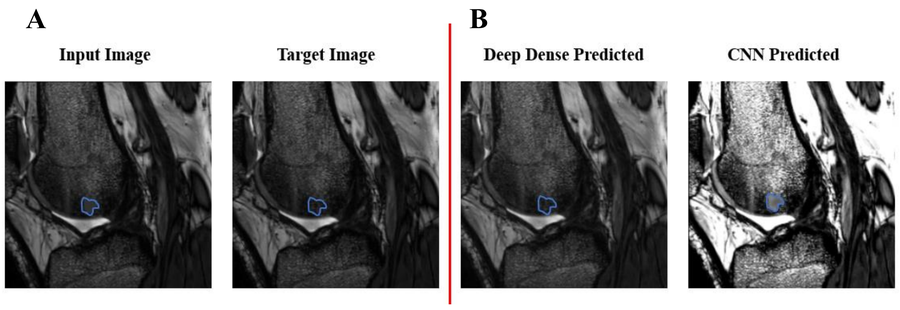


Figure 3. a) Input and target images; b) The predicted image (artifact correction by model)

## REFERENCES

[1] Haung X, et al. 2018. *BioMed Engineering OnLine*
[2] Smith TB, et al. 2010. *Imaging Med.*

## RESULTS

| Model | Percent Difference: Target Mean and Predicted Mean | P Value |
|---|---|---|
| Deep Dense | 0.17% | .77 |
| Shallow Dense | 2.26% | < .01 |
| CNN | 14.56% | < .01 |
| Composite | 2.77% | < .01 |

Figure 4. Target vs. Predicted Mean SI

- The Deep Dense model had the smallest percent difference between the target and predicted
  - The paired t-test showed that the difference was not significant
- To further evaluate the model, boxplots were plotted of the mean SI values for target and predicted artifact regions (Figure 4)
- CNN had a larger percent difference between the target and predicts image and the paired t-test showed that the difference was significant

## DISCUSSION

- A multilayer perceptron (MLP) is not usually ideal for most computer vision tasks. However, this study found the best model to be the Deep Dense model
- Deep Dense model had a p-value greater than 0.05 for the paired t-test and the target and predicted boxplots had very similar ranges
- The Deep Dense model images appeared visually well-corrected when compared to their target images
- It was expected that the CNN model would have the best success in removing artifacts as they are widely used for image/object recognition
- The CNN had trouble removing the artifacts, but enhanced the contrast of the images

Limitations:

- More training data may significantly improve the performance of the models
- During the training process the generated artifacts were limited in size and brightness

## CONCLUSION

- A variety of image-correcting models were evaluated using the artifact generator to create training data
- The Deep Dense model was most successful in correcting real artifacts, both statistically and visually
- Future work will further develop and train the models to complete image augmentation tasks

## ACKNOWLEDGEMENTS

Funded by the NIH (NIAMS R01-AR065462, NIGMS P30 GM122732), the National Football League Players Association, the Lucy Lippitt Endowment, the RIH Orthopaedic Foundation, and the Boston Children's Hospital Orthopaedic Surgery Foundation.

# Development and Clinical Evaluation of a Device for Measuring Weight Bearing in Pediatric Standers

Joseph Stevenson, Joseph Crisco, Ph.D.

UNIVERSITY ORTHOPEDICS
BROWN Department of Orthopaedics
Lifespan Orthopedics Institute
Rhode Island Hospital · The Miriam Hospital
Newport Hospital
*Delivering health with care®*

## Introduction & Aims

Assisted standing for children requiring wheelchairs for mobility has proven to be beneficial from both psychological and physiological perspectives. However, due to the current rigid design of standers, it has been demonstrated that children may not actually be fully weight bearing. The aim of this study is to develop a weight bearing device (WBD) to measure and better understand foot loads while in standers in order to assist caregivers in improving positioning as well as a more precise metric in studies of the benefits of standing.

## Methods

- Participants: After IRB approval, this study recruited 5 individuals, aged between 8 to 17 years old that utilize a stander in a school setting.
- Testing Protocol: Students were assisted into their stander (prone, vertical, or supine) and strapped in by a physical therapist. The weight bearing device was aligned under the student's feet and real-time data was streamed over a 20-minute interval. Postural and strap adjustments were made with help of the WBD and noted for future reference.
- Calibration Testing:
  - Point loading tests [0-150lbs] with an Instron machine confirmed that the board's accuracy was approximately 96% at the center, with decreasing accuracy as the load moved away from the center.
  - Used the most accurate data from the center of the board to create a calibration factor to calibrate millivolt readings across the entire board.
  - With help of a Bland-Altman plot, an analysis of the relationship between load data and calibrated data predicted the accuracy of the board to range between 65 to 70 lbs across all 11 locations before bias significantly increase (>5).

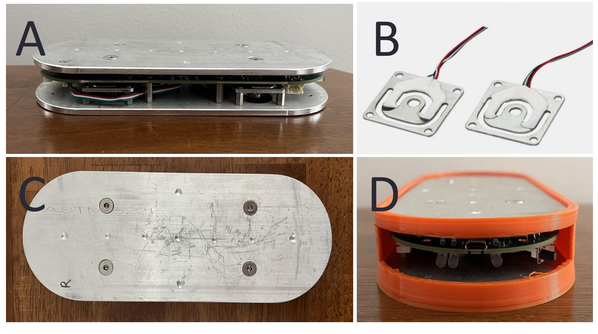


**Fig. 1**: Design of Weight Bearing Device
A. Right side view of device without protective gasket
(B) Galoce full-bridge micro load cell sensors, GM670
C. Top view of the device,
(D) Front view of the device, USB location for hardwiring.

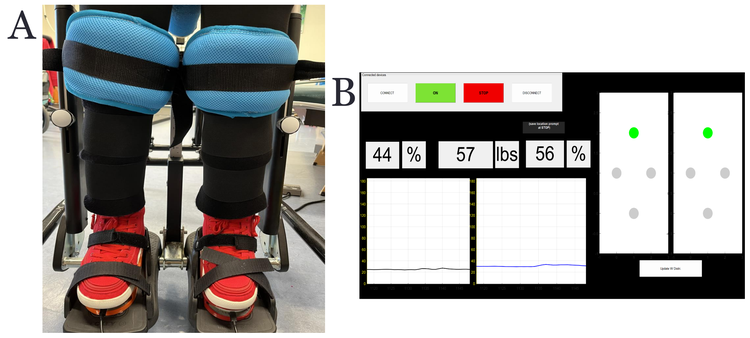


**Fig 2:**
A. Hardware setup with a child secured into their stander.
B. The corresponding weight bearing data collected from standing.

## Results

| | Initial Left % | Initial Right % | Expected Weight (lbs) | Initial Measured Weight (lbs) | Difference | Reduction in Weight Bearing % | Stander Type |
|---|---|---|---|---|---|---|---|
| **Subject 1** | 38% | 62% | 72 | 56 | 16 | 22.22 | Supine |
| **Subject 2** | 45% | 55% | 73 | 62 | 11 | 15.07 | Vertical |
| **Subject 3** | 53% | 47% | 65 | 52 | 13 | 20.00 | Prone |
| **Subject 4** | 55% | 45% | 71.4 | 25 | 46.4 | 64.99 | Supine offset 35 degrees |
| **Subject 5** | 46% | 54% | 75.4 | 51 | 24.4 | 32.36 | Prone |

**Table 1 :** Initial data points collected and calculated from all students.

| | Final Left % | Final Right % | Expected Weight (lbs) | Initial Measured Weight (lbs) | Difference | Reduction in Weight Bearing % | Maximum Weight Recorded (lbs) |
|---|---|---|---|---|---|---|---|
| **Subject 1** | 42% | 52% | 72 | 54 | 18 | 25.00 | 60 |
| **Subject 2** | 50% | 50% | 73 | 60 | 13 | 17.81 | 64 |
| **Subject 3** | 57% | 43% | 65 | 50 | 15 | 23.08 | 53 |
| **Subject 4** | 51% | 49% | 71.4 | 20 | 51.4 | 71.99 | 37 |
| **Subject 5** | 43% | 57% | 75.4 | 54 | 21.4 | 28.38 | 68 |

**Table 2 :** Final data points collected and calculated from all students. Recording of 'Maximum Weight' over the 20-minute interval.

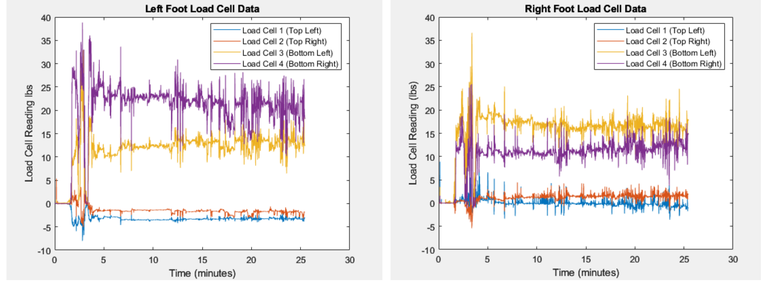


**Fig. 3:** Left and right load cell stream over 20-minute testing period from Subject 2

## Conclusions

The results to date have clearly demonstrated that the children are not fully weight bearing, but real-time adjustment in stander positioning and strapping can improve weight bearing. This information can be used by the physical therapists to correct straps tightness or brace locations to achieve a higher weight bearing load.

The results in Tables 1 and 2 highlight a notable discrepancy in measured weight (in pounds) when supine standers are offset from the vertical position, resulting in a reduction in weight bearing of 65% and 72%. Conversely, vertical standers consistently yielded the highest measured weight, with a difference in expected verse initial weight of only 11 and 13 pounds. For prone and supine stander types, the reduction in weight bearing falls within the range of 20-32%.

Throughout the testing sessions, various postural and strap adjustments were made to achieve greater weight bearing capabilities. These adjustments included re-aligning the feet on the force plates, and modifying the straps supporting the feet, pelvis and trunk. Visual cues, with help of the physical therapy staff and the assistance of the loading pattern tool, as depicted in Figure 2 of the graphical user interface, were instrumental in determining when these adjustments were necessary. The loading pattern tool utilizes the real-time millivolt readings to illustrate the type of loading occurring (posterior, medial, lateral, and anterior). Figure 3 provides a clear visualization of how we established this categorization by observing the load cells fire in pairs under the distributed loading conditions.

## Clinical Implications

Currently, physical therapists that utilize standers are unable to accurately tell how much the straps and braces are negatively affecting a patient's ability to optimally bear weight. The weight bearing device designed for this study supplies real-time data that can be used for improving therapeutic techniques and maximizing the health benefits from standing.

## Acknowledgements

This research was made possible by the students and physical therapists at Meeting Street.

# Responsiveness of ACL Cross Sectional Area to Oral Relaxin Administration

Zalk, S[1], Vaughan, Q[1], Yue, L[1], Owens, BD[1], Beveridge, JE[1]
[1]Department of Orthopeadics, Warren Alpert Medical School of Brown University and Rhode Island Hospital, Providence RI

## Introduction:

- Anterior cruciate ligament (ACL) injuries are more common in females than males[1] possibly due to sex-based hormones, including relaxin[2,3]
- Because the ACL is composed primarily of Type I collagen, it may be susceptible to the negative effects of relaxin resulting in diminished ACL stiffness and ultimate tensile strength[4]
- The Cross-Sectional Area (CSA) of an ACL is needed to calculate ultimate tensile strength.

## Hypothesis & Aims:

- Hypothesis: Oral relaxin administration reduces ACL biomechanical properties in a rodent model.
- Aim 1: In a pilot study, develop an optical method to quantify ligament CSA
- Aim 2: In an experimental study, determine whether CSA is affected by age/or relaxin treatment.

## Materials & Methods:

**Pilot Study:**

- Four Sprague-Dawley rats were used to develop the optical method for CSA measurement.
- Minimum ACL CSAs were calculated from diameters based on where the user believed to be the smallest width (Figure 1, 2)
- Average ACL CSAs were calculated from diameters measured at approximately 1/3, 2/3, and 3/3 of the visible longitudinal ACL (Figure 3, 4)

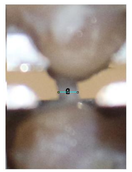

*Figure 1: Sagittal Plane (minimum)*

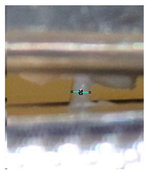

*Figure 2: Coronal Plane (minimum)*

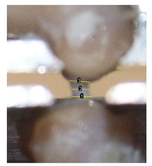

*Figure 3: Sagittal Plane (average)*

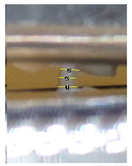

*Figure 4: Coronal Plane (average)*

## Materials & Methods (continued):

**Experimental Study:**

- Thirty-six female rats were tested, consisted of three equal groups: a control group, a group administered relaxin, and an aged group
- The specimens were tested on a universal testing machine with a 1kN load cell calibrated to a resolution of 0.056 N at a 10 N load (Figure 5)
- Images of the ACL were taken approximately 135mm away from specimen with camera set to auto-adjust shutter speed, aperture, and ISO with lens adjusted to a 135mm macro
- CSA calculated with diameters of ACL in coronal and sagittal planes

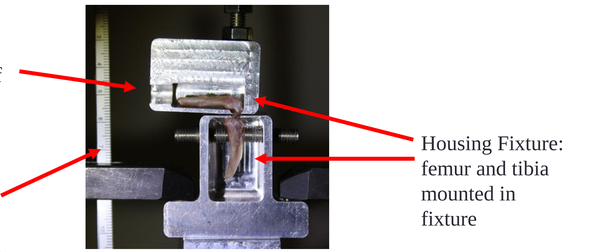


*Figure 5: Experimental Study Fixture*

**Data Analysis:**

- Pilot data were analyzed using inter/intraclass correlations and Bland-Altman plots with a bias of less than 10%

## Results:

**Pilot Study:**

- Minimum CSA approach was more robust and repeatable (Table 1)

| | Minimum CSA Measurements (mm²) | | | Average CSA Measurements (mm²) | | |
|---|---|---|---|---|---|---|
| Specimen | Initial Measurement | Follow-Up Measurement | % Difference | Initial Measurement | Follow-Up Measurement | % Difference |
| 1 | 1.03 | 1.10 | 6 | 1.36 | 1.51 | 10 |
| 2 | 0.65 | 0.64 | 1 | 0.76 | 0.82 | 7 |
| 3 | 0.82 | 0.90 | 9 | 1.04 | 1.11 | 7 |
| 4 | 0.55 | 0.51 | 7 | 0.89 | 0.69 | 29 |

*Table 1: Minimum and Average CSA Measurements*

- Differences between intra- and inter-user CSA were less than 10% (Table 2, 3)

| Intra-User Measurements | | | | |
|---|---|---|---|---|
| Specimen | 1 | 2 | 3 | 4 |
| Avg. Area (mm²) | 1.01 | 0.57 | 0.31 | 0.64 |
| Percent Difference | 3.02 | 1.07 | 1.65 | 9.40 |
| stdev Sagittal Measurements (mm) | 0.02 | 0.00 | 0.00 | 0.03 |
| stdev Coronal Measurements (mm) | 0.00 | 0.01 | 0.01 | 0.02 |

*Table 2: Intra-User CSA agreement*

| Inter-User Measurements | | | | |
|---|---|---|---|---|
| Specimen | 1 | 2 | 3 | 4 |
| Avg. Area (mm²) | 1.05 | 0.58 | 0.30 | 0.69 |
| Percent Difference | 9.92 | 1.70 | 1.87 | 4.76 |
| stdev Sagittal Measurements (mm) | 0.01 | 0.02 | 0.02 | 0.02 |
| stdev Coronal Measurements (mm) | 0.08 | 0.01 | 0.01 | 0.01 |

*Table 3: Inter-User CSA agreement*

## Results (continued):

- The administration of relaxin had no effect on CSA (Figure 6)
- Load-Displacement curves were inspected visually to ensure symmetry bilaterally and to confirm that structural properties could be extracted (Figure 7)

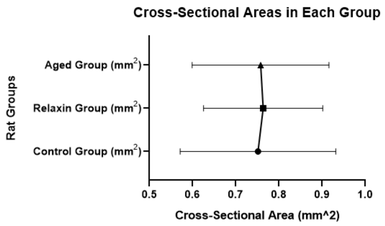


*Figure 6: CSA of Experimental Study Groups*

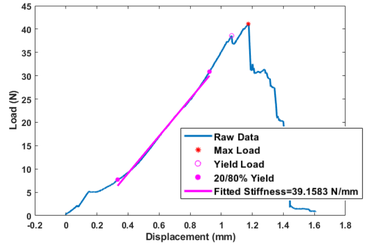


*Figure 7: Load-Displacement Sample*

## Conclusion:

- CSA calculated from the minimum diameter approach was more robust and will be applied to determine ACL ultimate tensile strength
- The similarity in CSA across experimental groups suggests that CSA was not responsive to oral relaxin administration

## Clinical Implications:

If relaxin administration diminishes ACL biomechanical properties, future treatments that target relaxin could reduce female ACL injury risk

## References:

1-Gilmer et al. JB JS Open Access. 2020 Feb 21;5(1). 2-Konopka et al. Am J Sports Med. 2020 Jan;48(1). 3-Bani et al. Gen Pharmacol. 1997 Jan;28(1). 4-Markatos et al. Eur J Orthop Surg Traumatol. 2013 Oct;23(7).

## Acknowledgements:

This work was supported by NIH NIAMS (K99/R00-AR069004, R01-AR047910, R01-AR074973) and NIGMS (P30-GM122732, P20-GM139664)